Young's fringes from vertically integrated slab waveguides: Applications to humidity sensing

Graham H. Cross, Yitao Ren, and Neville J. Freeman

Citation: Journal of Applied Physics **86**, 6483 (1999); doi: 10.1063/1.371712
View online: http://dx.doi.org/10.1063/1.371712
View Table of Contents: http://scitation.aip.org/content/aip/journal/jap/86/11?ver=pdfcov
Published by the AIP Publishing

Young's fringes from vertically integrated slab waveguides: Applications to humidity sensing

Graham H. Cross[a] and Yitao Ren
Department of Physics, University of Durham, South Road, Durham DH1 3LE, United Kingdom

Neville J. Freeman[b]
Farfield Sensors Limited, Unit 51, Salford University Business Park, Leslie Hough Way, Salford, Greater Manchester M6 6AJ, United Kingdom

(Received 17 December 1998; accepted for publication 26 August 1999)

Using a multiple layer optical waveguide system consisting of two vertically slab waveguides, classical Young's fringes may be obtained in the far-field diffraction plane. In agreement with the simple theory of diffraction interference the spacing of the far-field fringes is easily observed on mm to cm dimensions without further transformation of the output light. The simple methods of fabrication and means of optical coupling should provide a readily adaptable method for examining the principles of interferometry in an integrated optical format. The structure acts to transform polarized incident plane wave input light into separate slab modes of the device which emerge as two closely spaced and coherent sources at the output. The elements required for a classical Young's fringe demonstration are therefore all embodied in this approach. The basic concept can be applied to an optical method for sensing. In one example of this we demonstrate measurement of the phase difference induced between the upper and lower propagating modes in structures due to water vapor diffusion into the layers which are formed from hydrophilic polymers. The Young's fringe patterns exhibit a spatial intensity distribution which is sensitive to water vapor introduced over the surface of the structure. Differences in the effective index between the modes of the two waveguides during the diffusion of the vapor causes phase shifts which result in redistribution in the fringe pattern. The anticipated limit of detection of these devices is lower than 1 ppm for water vapor. © *1999 American Institute of Physics.* [S0021-8979(99)03823-2]

I. INTRODUCTION AND RATIONALE

Optical methods of detection for gases and vapors can utilize a range of optical response functions the most general of which is a change in the refractive index of the sensing material. Interferometry can then be used to detect the induced phase changes of the propagating light. Optical waveguide formats can offer a compact system yet are often rather complicated in their design and operation. It would be desirable to remove many of the optical transforming components in the system (such as lenses and polarizers) and remove the need for precise alignment of source and detectors with the waveguide. Furthermore, in many interferometer designs, such as in the directional coupler or Mach-Zehnder modulator, it is necessary to carefully control the dimensions to provide a device which may operate at its most sensitive point (the ''quadrature'' point). This latter problem is overcome if the complete optical transfer function is available for interrogation. In a two-dimensional interference pattern this is the case and the device described here provides such a pattern.

In general, two identical transverse waveguide modes are used to provide the interference necessary to detect phase shifts. One mode acts as a reference against which phase shifts induced in the other can be measured. A differential change in the mode effective indexes is required to produce the interferometry to be measured. The most obvious example where this has been demonstrated for vapor sensing is in Mach-Zehnder (MZ) type designs.[1–3] The two arms of the MZ interferometer each carry a single mode, one of which is perturbed by the test vapor before it recombines with the other to produce an intensity modulation in the output waveguide. Among other problems, the planar waveguide Mach-Zehnder interferometer is quite demanding of fabrication tolerance. Ideally, the device would be fabricated with a $\pi/2$ phase bias built into the structure. If not, then some means of externally biasing the device is necessary to achieve the optimum sensitivity. Such tolerance is not generally possible on a routine basis. This is equally true of the planar directional coupler designs. In both cases, it is the intensity modulation in the near-field output of a single channel waveguide which is measured and thus the light must be collected from a spatial region with the dimensions of the waveguide, i.e., on the order of a few μm^2. Optical fibre coupling is usually the most convenient method.

Methods which rely on modulation of a far-field intensity pattern may also be considered.[4,5] Far-field interferometry may utilize either of two classical principles: Fraunhofer diffraction, in which the diffraction from a single aperture creates a pattern and Young's fringe interference where in the far-field, essentially cylindrical waves emanating from two closely spaced apertures create a simple pattern of

[a]Electronic mail: g.h.cross@durham.ac.uk
[b]Electronic mail: neville.freeman@farfieldsensors.freeserve.co.uk

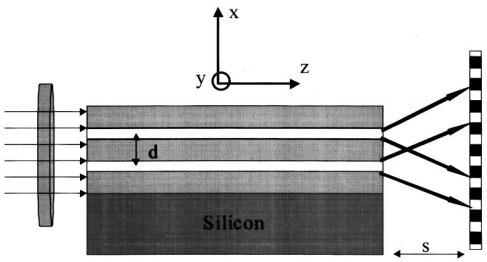

FIG. 1. Schematic diagram of the multiple stack slab waveguide sensor chip and method of optical coupling. Vapor enters through the top surface and diffuses through the structure. In the preferred design, the central cladding layer is of a material that is impervious to the analyte vapor.

fringes. These methods have inherent advantage in that the absolute sign of induced phase changes can be determined during sensing and, furthermore, it is possible to directly correlate changes in position of the pattern with phase changes in a linear way.

Many methods of optical waveguide sensing rely on the interaction of the analyte with a sensing layer acting as an optical cladding layer to the waveguide. The guided modes are perturbed through the interaction with the evanescent field of the modes.[6–9] An immediate advantage in sensitivity is to be gained if the whole of the guiding layer can act as the sensing medium since most of the optical field lies within the guiding region. This has been recognized and devices where the waveguide layer itself is the sensing element have been demonstrated.[10–12]

We report on a system in this work which combines these two advantages. We have fabricated a multiple layer waveguide system, comprising two vertically displaced slab waveguides. Optical coupling to the modes of the structure is made by uniformly illuminating the input end face of the sensor with a coherent laser source. The structure spatially filters the light to produce two discrete distributions of optical power propagating in the slab waveguide modes which emerge as two closely separated sources at the sensor output end-face. Young's fringes are measured in the far-field due to diffraction from the two closely spaced apertures. The unusual feature of this device is the vertical stacking of the waveguides which allows one to choose the two waveguide layers not only for their optical properties but also for their selective response to vapors. The lower layer can be chosen to be insensitive to the analyte or a separating layer can be chosen which is impervious to the analyte. In either case one obtains sensing and reference waveguides without the common difficulties of patterning of structures in the single waveguide plane.

II. OPTICAL THEORY

A. Waveguide coupling and propagation

The waveguide structure consists of two vertically stacked slab waveguides (see Fig. 1.) The modes of the structure may be calculated for each polarization [transverse electric (TE) or transverse magnetic (TM)] by considering confinement boundaries only in the x direction (referring to Fig. 1). In our calculations, the silicon layer is neglected since the program cannot compute the radiation modes applicable to a high refractive index semi-infinite medium such as silicon. In practice, this layer will act as a source of uniform propagation loss for the less well confined modes. The semi-infinite medium above the upper cladding layer is taken to be air with a refractive index of unity.

TABLE I. Structural and optical properties applied to the calculation of the fields in the all-polymer structure.

Layer	1	2	3	4	5	6
Thickness (μm)	3	0.7	2.65	0.7	3	∞
Refractive Index	1.49	1.57	1.49	1.57	1.49	1

At this point we will define the two structures to be discussed. The first (the ''all-polymer'' structure) consists of a stack of polymer layers on the silicon substrate consisting of only two types of polymer material. The second (the ''hybrid'' structure) consists of a silicon dioxide layer on the silicon substrate onto which a further series of polymer layers is deposited. Calculations of the general structure of Fig. 1 (either all-polymer or hybrid) yield supermodes as solutions, with fields extending through the thickness of the structure. Depending on the precise design, modes may be found which will in practice be lossy since they are not well confined in the core layers. Such modes may be referred to as ''cladding'' modes. Furthermore, where the design represents a symmetrical arrangement between the lower and upper cladding layers (i.e., similar thickness of core layers in an all-polymer structure) the two lowest order supermodes are nearly degenerate and each consists of two well separated lobes of field confined in the core layers. To illustrate this we list in Table I the parameters used to calculate the modes of the all-polymer structure considered experimentally in Secs. III and IV. The layers are considered to be lossless media. In Table II we present the calculated effective indexes of the supermodes of the structure for the two polarizations. Notice that the two highest order modes have effective refractive indexes that are close to that of the cladding material index. While these modes will be excited in the structure under the uniform illumination of the source, they will in practice experience much higher loss than the two lowest order modes which are strongly confined to the core layers. In practice it is extremely difficult to fabricate a structure which is exactly symmetrical since we can control layer thickness only to around ± 0.1 μm. In these cases, and in all other cases where we deliberately fabricate asymmetrical structures, the two lowest order modes are represented not by supermodes but by the two lowest order modes of the separate slab waveguides.

TABLE II. Effective refractive indexes calculated for the all-polymer structure using a wavelength of 632.8 nm.

Mode	0	1	2	3
TE	1.544 946 73	1.544 946 12	1.491 781 12	1.490 829 40
TM	1.543 446 49	1.543 445 76	1.491 549 63	1.490 557 36

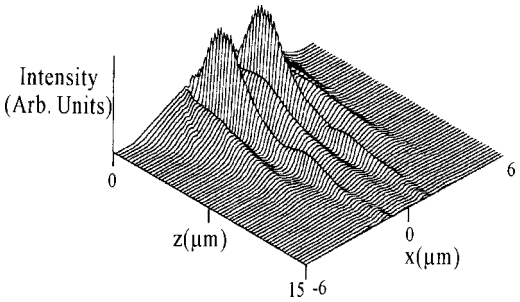

FIG. 2. Propagation of the field intensity in two vertically stacked slab waveguides. The transverse direction is shown along *x* and the propagation direction is along *z*.

If the two lowest order waveguide modes can be excited simultaneously and with equal efficiency, fringes with the highest contrast can be obtained (assuming also that the propagation losses are identical in the two guides). This aspect of the design represents a significant departure from conventional waveguide applications where precise alignment between source and guide is usually required (as in fibre coupling, for example). The positional tolerance on input coupling is lowered to above many tens of microns in the input plane if a diode laser source is placed 1–2 mm from the end-face. The cross-section of the input beam is large compared to the dimensions of the waveguide stack. This guarantees almost equal coupling efficiency to modes of identical cross section even if the source and waveguides are misaligned from device to device. The efficiency of coupling (source to modes) will obviously be very low but in our experience this is not a problem for the sensitivities of commercially available silicon photodiode detectors after propagation and diffraction of the out-coupled light.

The results of a numerical computation of the evolution of the TE field with propagation is shown in Fig. 2 over a propagation distance of 15 μm. The starting field distribution is a circular Gaussian having an intensity half-width of 5 μm and a free space wavelength of 0.6328 μm. The refractive index distribution is modeled as two rectangular regions with a refractive index of 1.57. The width (*y* direction) of the regions is set such that the width of the propagating field is well within the bounded region and therefore simulates the lack of confinement in the *y* direction. The height of the regions is 0.7 μm to simulate the thickness of the layers used in experiments. The waveguide layers are separated between the guide centers by 3.6 μm. The height and separation are similar to the dimensions of the all-polymer waveguides used in the experimental work. The refractive index difference between the core and cladding is 0.08. A layer of refractive index of unity (air) is included on one surface of the structure. Thus the structure is identical in cross section to that described by the parameters in Table I from which the exact waveguide modes were calculated.

There is an overall intensity reduction in the field with propagation distance (shown in Fig. 2) which is due to diffraction in the plane of the waveguide (where the field is unconfined). In the vertical (*x*) direction, however, the field redistributes slowly into two well separated peaks of intensity representing the power contained in the two lowest order supermodes of the structure. After a propagation of 120 μm the field intensity distribution in the *xy* plane has evolved into two main lobes confined to the two slab guides as shown in Fig. 3.

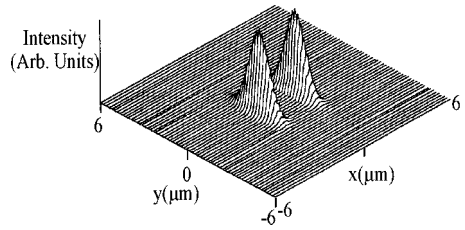

FIG. 3. Calculated field intensity distribution in the *xy* plane of the device after a propagation distance of 120 μm.

B. Far-field pattern

The intensity distribution in the far-field will represent the interference between the two fields emanating from the waveguide 'slit' apertures. On the conventional Huygens model each waveguide will act as a source of cylindrical waves diffracting into the far-field where they will overlap to give Young's interference fringes.

We analyze this problem by numerically computing the diffraction of the field calculated previously at the device output face. Figure 4 shows the fringes calculated by propagating the fields over a distance, *s*, of 1 cm.

The full spatial intensity pattern is described by a set of fringes modulated in the *x* direction and contained within a Gaussian envelope which results from diffraction. According to the simple theory of interference fringes maxima and minima of intensity should be spaced with spacing, *a*, according to

$$a = \frac{\lambda s}{d}, \tag{1}$$

where λ is the wavelength (632.8 nm in this case) and *d*, the separation of the sources.

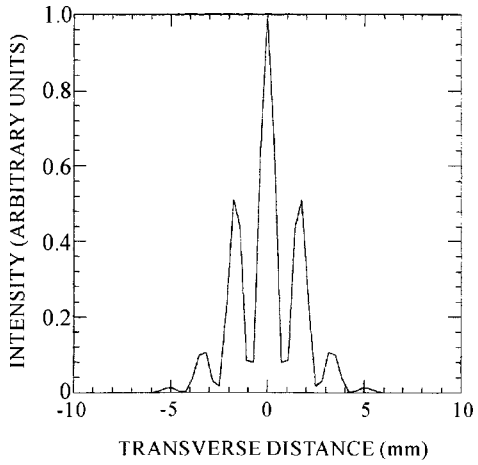

FIG. 4. Transverse section through the calculated far-field fringe pattern at a distance $s = 1$ cm.

It is interesting to note that the close spacing of the sources in this structure ($d=3.6\ \mu$m) leads to fringes whose separation is clearly observable on centimeter dimensions without a lens.

III. EXPERIMENT

A. Preparation of substrates

1. All-polymer structures

Poly(methyl methacrylate) (PMMA), (Polysciences Ltd.) was deposited onto bare silicon (100) wafers either by dip coating it from solutions in dichloromethane or by spin coating from solutions in chlorobenzene. For dip coating a concentration of 275 mg/ml was prepared whereas for spin coating the concentration was 286 mg/ml. Solutions of poly(4-vinylpyridine) (P-4VP) (M wt 60 000, Aldrich Co.) for dip coating were prepared and had a concentration of 90 mg/ml. Drying at lower temperatures ($<60\ ^\circ$C) in the later stages of deposition was found to reduce the stress crazing that was found otherwise.

2. Hybrid structures

In these structures one or more of the lower layers may be fabricated from silicon oxide or silicon oxynitride. In these initial studies we used substrates with a 1 μm layer of SiO_2 ($n=1.46$) as the lower cladding layer. The second and fourth waveguide layers were the water sensitive polymer, P-4VP ($0.9-1\ \mu$m, $n=1.57$) whilst the central layer was a commercial polyolefin polymer (Zeonex 480R, Nippon Zeon) with a thickness between 2.5 and 2.8 μm ($n=1.52$). This layer is impervious to water vapor and acts to isolate the lower P-4VP layer from water taken up in the top waveguide layer. No extra top cladding layer was used (i.e., we take the air to be the top cladding layer).

B. Optical studies

Short lengths (approx 10 mm) of waveguide substrate were formed by cleaving of the silicon wafer substrate. The polymer layers fracture along the line of the cleavature in favorable cases but it is known that this method can produce uneven polymer end-faces (see Fig. 5). Light from a helium neon laser was focused onto the input end-face of the waveguide using a microscope objective lens. The propagated light was then allowed to diffract out from the output face of the guide and onto either a screen or a camera, for direct observation, or onto a pinholed silicon photodiode. A chopper and lock-in amplifier may be used to smooth out the responses although it is clear that quite large changes in fringe intensity are readily produced and might be recorded directly.

C. Gas flow arrangements

A system in which two flasks are connected by a thin capillary tube was used which provides a calibrated test vapor.[13] The lower flask is held in a temperature controlled water bath and contains the reservoir of analyte liquid. In the upper flask, the carrier gas is passed through at fixed flow rates and dilutes the analyte vapor before passing on to the sample chamber. This equipment may be calibrated by measuring the weight loss of solvent from the lower flask for various flow rates of carrier gas (dry nitrogen) and at various temperatures. By using connecting tubes with an inner diameter of 5 or 2 mm (for the lower concentrations) between the upper and lower flasks it was possible to obtain calibration curves corresponding to the temperature and flow rate. Concentrations of water vapor of between 30 and 1000 ppm were produced.

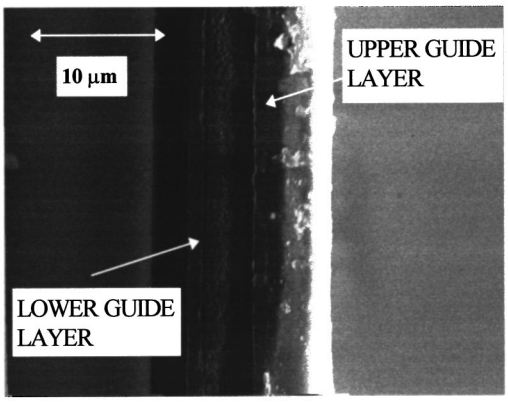

FIG. 5. Scanning electron microscope image of the end-face of a five-layer all-polymer structure. The individual polymer layers are clearly visible. The bright line at the right is due to charging on the nonconducting polymer top layer.

IV. RESULTS AND DISCUSSION

A. All-polymer structures

Clearly observable Young's fringes were seen in these structures although the images contain distortions due to both fabrication imperfections and consequences of the diverging source beam. The pattern also contains closely spaced vertical lines of intensity within each fringe which are attributable to fabrication imperfections including end-face preparation. Improvements to film quality (uniformity of thickness and index) and in end-face preparation should reduce this problem.

The sensitivity to water vapor was determined using the calibrated gas flow apparatus described above. The output from the sensor was allowed to fall onto a diffuser screen which smoothed out the fine structure of the interference pattern, particularly with regard to the vertical patterns which overlaid the Young's fringes. A Hamamatsu camera was used to record the vertical cross section of suitable parts of the pattern.

To analyze the phase shifts in the sensor we note that there is a linear relationship between position and phase and we can thus find the relative position shift, Δx of the fringe maxima in terms of the relative phase shift, $\Delta\varphi$ through

$$\Delta\varphi=\frac{2\pi\Delta x}{a}. \tag{2}$$

The phase shift observed was on the order of $\pi/3$ (0.94 rad) for a flow rate (40 ml/min) and temperature which should give 150 ppm of water vapor over the sample. At a slower flow rate the concentration of water can be increased. The

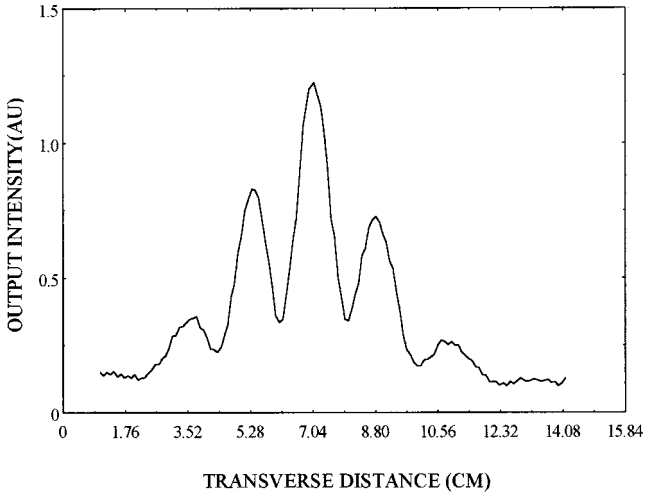

FIG. 6. Measured vertical intensity distribution of fringes produced from a ''hybrid'' system at a distance from the device end-face of 9.6 cm.

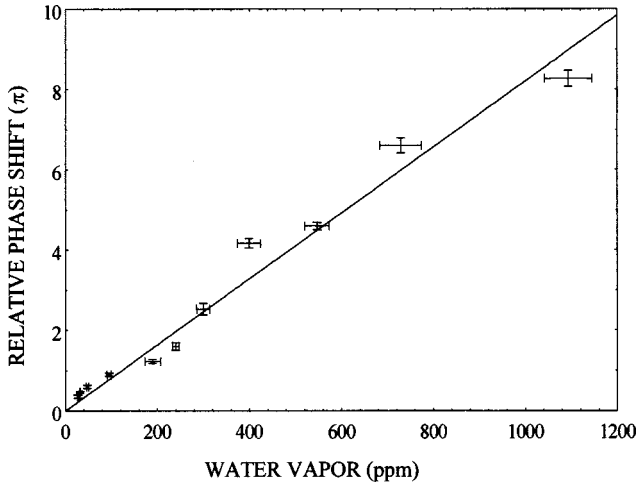

FIG. 7. Relative phase shift vs humidity concentration for a ''hybrid'' device.

response of the device to a flow rate of 10 ml/min, which is expected to deliver a concentration of 600 ppm to the sample, was $\pi/2$ (1.57 rad).

These responses, although reversible, clearly do not show a simple linear dependence of phase shift versus concentration. The sensitivity, furthermore, is rather low.

These all-polymer structures consist of two identical slab waveguides comprising hydrophilic polymers for both the cladding and the guide layers. This will complicate the response to vapors since vapor will quickly distribute through the whole of the structure with a final concentration gradient with thickness which could be quite small. The field in the lower waveguide will thus have its phase retarded in a similar way to that in the waveguide above, thus giving only a small net phase difference.

B. Hybrid structures

Fringes obtained experimentally from a typical hybrid structure are shown in Fig. 6. To confirm the Young's fringe condition [Eq. (1)] an intensity scan was taken through the cross section of a set of fringes. At a distance to the screen, *s*, of 9.6 cm we observed a separation between adjacent fringe maxima, *a*, of 1.76 cm. At a wavelength of 632.8 nm this gives a waveguide center separation for this sample, *d*, of 3.45 μm. This compares extremely favorably with the expected separation of between 3.4 and 3.8 μm and is thus within experimental error.

In the present configuration, these hybrid structures comprise a lower cladding layer of silicon dioxide, followed by three polymer layers. The central (polyolefin) layer of these three is designed to provide an impermeable barrier to water vapor and thus provide a dual slab waveguide structure wherein the upper layer is the sensing waveguide and the lower layer is the reference waveguide.

In these structures we have measured a nearly linear phase change response to water vapor concentrations from above 1000 down to 30 ppm (see Fig. 7). The lower limit is determined by our simple manual method of observing fringe shifts as described in Sec. IV A. Greater precision could be obtained by scanning the whole pattern using a linear array photodiode and calculating the accumulated phase shift. This method is used in the prototype commercial instrument.[14] Comparing the response of this structure to the all-polymer structure at 600 ppm, we see that whereas the all-polymer structure achieves only a $\pi/2$ phase shift (1.57 rad) the hybrid structure accumulates around 5π (16 rad) of phase. These hybrid devices are thus one order of magnitude more sensitive. We are developing a data logging algorithm for these sensors which will offer measurement resolution of better than 0.01 rad of phase. This corresponds to a detection limit in the current structures of around 400 ppb.

The sorption of vapor into the polymer matrix might be analyzed using the Clausius–Mossotti formalism for a composite material but we do not propose to invoke this analysis with its associated uncertainties. Instead, a simple constitutive model for the refractive index of the polymer may be applied if the assumption is made that, in this concentration range, the water enters the polymer's free volume without causing swelling.[15] In glassy polymers such as PMMA and P-4VP the free volume fraction is on the order of a few percent of the total polymer volume but is known to be a quantity which is a product of the thermal history of the polymer. Our model thus considers that the refractive index of the polymer is made up of the intrinsic refractive index of the polymer chains, the refractive index of the free volume fraction ($n \approx 1$), and the refractive index of water. Clearly we are neglecting the influence of the Lorentz-Lorenz local field factors which would modify the analysis somewhat. Occupation of the accessible free volume by water will induce a change in the overall refractive index of the polymer film, Δn, according to the following formula:

$$\Delta n = (n_g - 1) f \tag{3}$$

where n_g is the guest species index in its condensed phase ($n_g \approx 1.33$ for water) and f contains all the information regarding the partitioning of water from the mobile phase into the polymer film. Notice that since the water simply displaces air in the free volume fraction the sensitivity to overall index change is related simply to the index difference

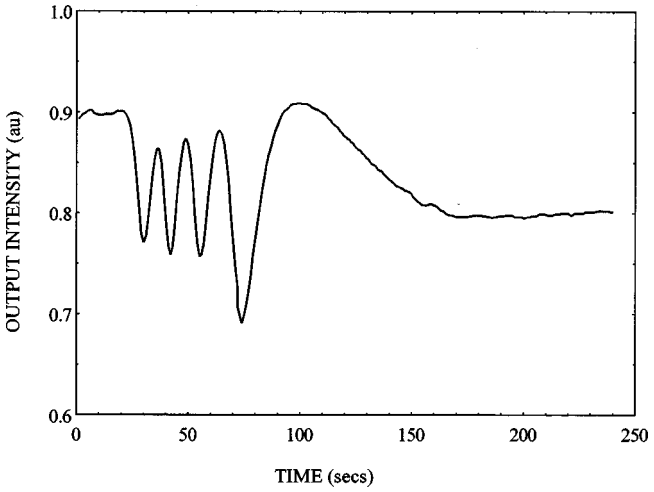

FIG. 8. Response of the ''hybrid'' structure to 1100 ppm of water vapor as a function of time. The measured response is taken from a point in the vertical intensity distribution using a pinhole photodiode.

between water (in this case) and air. This model differs from alternative suggestions where it is assumed that the vapor taken up by the polymer acts as the second component of a two component solution.[1]

The sensitivity, *f*, will include the solubility of the analyte in the stationary phase (characterized by a sorption coefficient). Some weak hydrogen bonding is possible in P-4VP and dipole/dipole interactions may also play a role since the dipole moment of the pyridine group is around 2.2 D. The data of Fig. 7 may be fit to a straight line but we point out that an apparent periodicity in the response might be interpreted from the data. We believe this to be associated with an experimental artifact whose origins are being explored at present. Notwithstanding this, we obtain a slope value for *f* of 0.8, which is the combination of the sorption coefficient and the accessible free volume fraction. The latter is largely a function of the thermal history of the polymer but is on the order of a few percent.

An impression of the speed of response can be seen in the pinhole detected intensity versus time to exposure of 1100 ppm of water vapor (Fig. 8). At $t=0$ the valve is operated and the observed time delay before the onset of the response is governed by the flow rate, the length of the tube leading to the sample chamber, and the remaining ''dead volume'' in the equipment. The sample then responds to the vapor to produce around 9π of phase shift and the time taken to reach equilibrium is around 150 s. This response time is found to be largely independent of the partial pressure of water in the mobile phase which implies that the dynamics for mass transfer follow simple rules.[16]

V. CONCLUSIONS

Multiple layer slab waveguides fabricated in polymer on silicon wafer substrates have been demonstrated. A theoretical description of the optical properties of the structures has been verified through experimental observations. The feasibility of a sensing function for vapors has been demonstrated in two types of structure investigated. In the case of structures comprising two vertically adjacent slab waveguides we have observed that water vapor, diluted to a few tens of ppm in dry nitrogen, can enter the structure and produce refractive index changes that are sufficient for measurement of intensity fringe shifts in a far-field Young's fringe pattern. The fringe shifts are reversible over many cycles and the effects show a rapid response after taking account of the vapor delivery apparatus.

The optical structure and the far-field measurement described allows the analysis of the sign as well as the magnitude of phase changes in response to vapor. In principle, there is extra information on the relative loss between the sensing and reference waveguides. Changes to the fringe intensity contrast could add to the phase information provided and give further information as input to an intelligent postprocessor.

One of the main obstacles to commercial implementation of integrated optical sensors, that of optical coupling to the sensing structure, is removed in this design.[17] The wide tolerance to misalignment of source and detector with the sensor substrate is a unique feature of the present devices. There is considerable scope for further development of these basic operating principles and many possible engineering methods which could lead to a low cost packaged device. The method can be readily reproduced using simple sequential layer deposition methods from a wide variety of materials. We therefore would encourage not only commercial but also educational use of the concept due to the scope for rugged samples and easily demonstrated principles of interferometry.

ACKNOWLEDGMENTS

The authors are grateful to Dr. D. Wood (School of Engineering Science, University of Durham) for supplying the oxidized silicon wafers. They thank S. Harris (Zeon Chemicals Europe Ltd.) for the supply of Zeonex 480R.

[1] N. Fabricus, G. Gauglitz and J. Ingehoff, Sens. Actuators B **7**, 672 (1992).
[2] A. Brandenburg, R. Edelhauser, and F. Hutter, Sens. Actuators B **11**, 361 (1993).
[3] R. G. Heidemann, R. P. H. Kooyman, and J. Greve, Sens. Actuators B **10**, 209 (1993).
[4] A. Brandenburg and R. Henninger, Appl. Opt. **33**, 5941 (1994).
[5] R. Kherrat, N. Jaffrezic-Renault, P. Greco, H. Helmers, P. Benech, and R. Rimet, Sens. Actuators B **37**, 7 (1996).
[6] X. M. Chen, D. K. Qing, K. Itoh, and M. Murabayashi, Opt. Rev. **3**, 351 (1996).
[7] A. Klotze, A. Brecht, and G. Gauglitz, Sens. Actuators B **39**, 310 (1997).
[8] E. F. Schipper, A. M. Brugman, C. Dominiguez, L. M. Lechuga, R. P. H. Kooyman, and J. Greve, Sens. Actuators B **40**, 147 (1997).
[9] B. F. Schneider, J. G. Edwards, and N. F. Hartman, Clin. Chem. **43**, 1757 (1997).
[10] K. H. Kim, H. Minamitani, H. Hisamoto, K. Suzuki, and S. W. Kang, Anal. Chim. Acta **434**, 199 (1997).
[11] W. Lukosz and C. H. Stamm, Sens. Actuators A **25–27**, 185 (1991).
[12] R. E. Kunz, C. L. Du, J. Edlinger, H. K. Pulker, and M. Siefert, Sens. Actuators A **25–27**, 155 (1991).
[13] J. M. McKelvey and H. E. Hoelscher, Anal. Chem. **29**, 123 (1957).
[14] Analight EVA/500 vapor detection system (Farfield Sensors Ltd.).
[15] W. Lukosz, Sens. Actuators B **29**, 37 (1995).
[16] *International Encyclopaedia of Heat and Mass Transfer*, edited by G. F. Hewitt, G. L. Shives, and Y. V. Polezhaev (Chemical Rubber, New York, 1997).
[17] N. J. Freeman and G. H. Cross, Int. Patent No. 98/22807 (28 May 1998).